Biomolecules and Biomedicine
ISSN: 2831-0896 (Print) | ISSN: 2831-090X (Online)
Journal Impact Factor® (2024): 2.2
CiteScore® (2024): 5.2
www.biomolbiomed.com | blog.bjbms.org

SUPPLEMENTAL DATA

Quinuclidin-3-one-based quaternary ammonium compounds as potent antibacterials against *Staphylococcus aureus* and *Listeria monocytogenes*

Antonio Sabljić[1], Doris Čarija[1], Karolina Begić[2], Renata Odžak[1], Rozelindra Čož-Rakovac[2], Josip Tomaš[1], Matilda Šprung[1*]

[1]Department of Chemistry, Faculty of Science, University of Split, Split, Croatia;

[2]Ruđer Bošković Institute, Laboratory for Biotechnology in Aquaculture, Division of Materials Chemistry, Zagreb, Croatia.

***Correspondence to **Matilda Šprung**: msprung@pmfst.hr

Full article is available at the following link: Quinuclidin-3-one-based quaternary ammonium compounds as potent antibacterials against *Staphylococcus aureus* and *Listeria monocytogenes*

General Information

^{1}H NMR and ^{13}C NMR spectra were recorded using a Bruker Avance AV600 spectrometer operating at 600 MHz (^{1}H) and 150 MHz (^{13}C) at room temperature (298 K). All compounds were dissolved in $CDCl_3$; chemical shifts (δ) are reported in ppm relative to the residual solvent signal ($CDCl_3$: ^{1}H δ 7.26 ppm, ^{13}C δ 77.16 ppm). Coupling constants (J) are reported in Hz. High-resolution mass spectra (HRMS) were acquired on a Sciex TripleTOF 6600+ instrument (LC/MS QTOF) using electrospray ionization in positive mode (ESI^{+}). Spectra were processed and exported as PNG images.

Table S1. Statistical summary of PI uptake kinetics

Compound	Conc.	Fmax (a.u.)	tpeak (min)	Initial rate (a.u./min)	F at t=340 min (mean±SEM, a.u.)	AUC (a.u.·min ×10⁶)
QO-C₁₂	4×MIC	22,419	20	495.4	15,354 ± 327	5.98
	2×MIC	12,523	180	57.4	10,293 ± 601	3.31
	MIC	3,265	320	−7.1	3,074 ± 129	0.48
	½×MIC	1,131	20	9.1	−1,513 ± 372	−0.07
QO-C₁₄	4×MIC	24,418	20	532.1	12,871 ± 334	5.82
	2×MIC	7,005	300	13.4	6,654 ± 158	1.61
	MIC	5,393	260	6.9	4,794 ± 85	1.28
	½×MIC	580	0	−16.8	−802 ± 320	−0.17
QO-C₁₆	4×MIC	42,056	40	1036.9	37,638 ± 349	12.82
	2×MIC	30,051	260	543.0	29,997 ± 405	9.05
	MIC	25,485	320	542.0	25,422 ± 204	8.01
	½×MIC	**22,718**	**20**	**548.3**	**21,494 ± 91**	**7.23**

Statistical parameters of PI uptake kinetics in *Staphylococcus aureus* ATCC 25923 were assessed following exposure to QO-C_{12}, QO-C_{14}, and QO-C_{16} at four concentrations (4×MIC, 2×MIC, MIC, and ½×MIC) over a duration of 340 minutes. Bacterial suspensions (OD_{600} = 1.5 in PBS) were treated with 21 nM PI at 37 °C, with fluorescence monitored at 10-minute intervals (excitation at 536 nm, emission at 617 nm). Background fluorescence was subtracted from the measurements. F_{max} denotes the maximum fluorescence achieved during the observation period; *t_peak* indicates the time at which maximum fluorescence was recorded; the initial rate is represented by the linear slope calculated over the 0–40 minute interval; and F at t = 340 is the endpoint fluorescence (mean ± SEM, n = 3 independent biological replicates). The area under the fluorescence-time curve (AUC) was computed using the trapezoidal method over the 0–340 minute timeframe. Notably, red shading highlights the effect of QO-C_{16} at ½×MIC, which resulted in significant sub-MIC membrane disruption, while all other ½×MIC treatments exhibited no significant PI uptake above background levels. **Abbreviations**: ATCC, American Type Culture Collection; AUC, area under the fluorescence–time curve; a.u., arbitrary units; Conc., concentration; Fmax, maximum fluorescence; MIC, minimum inhibitory concentration; nM, nanomolar; OD_{600}, optical density at 600 nm; PBS, phosphate-buffered saline; PI, propidium iodide; QO-C_{12}, N-dodecyl-3-oxoquinuclidinium bromide; QO-C_{14}, N-tetradecyl-3-oxoquinuclidinium bromide; QO-C_{16}, N-hexadecyl-3-oxoquinuclidinium bromide; SEM, standard error of the mean; t_peak, time to peak fluorescence.

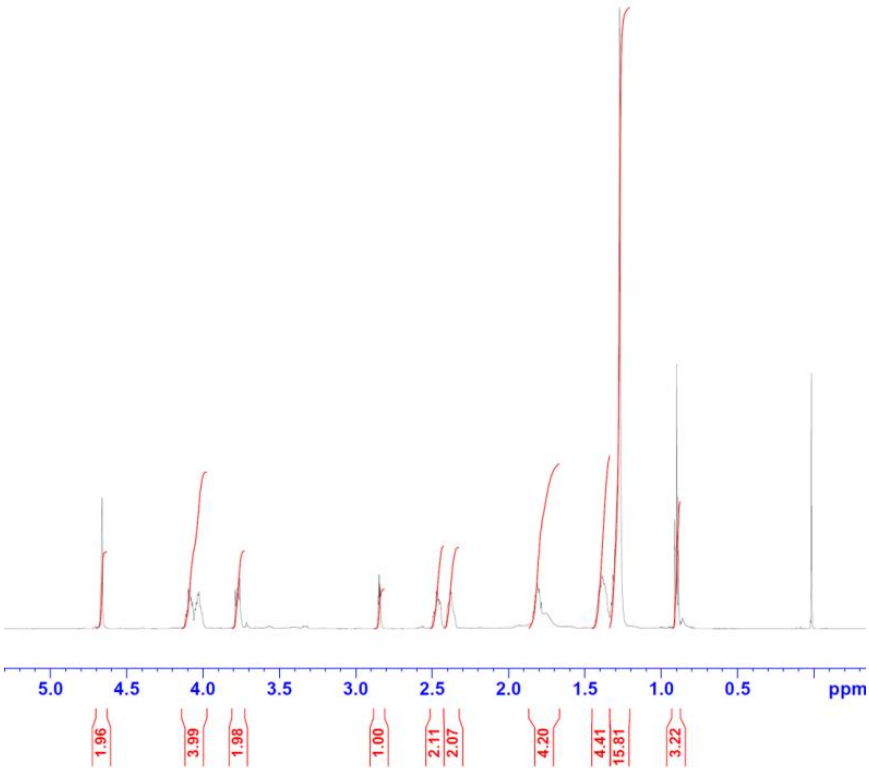


Figure S1. ^{1}H NMR spectrum of QO-C$_{12}$. Representative ^{1}H NMR spectrum of QO-C$_{12}$ recorded at 600 MHz in $CDCl_3$ at 298 K, with chemical shifts referenced to residual $CHCl_3$ at δ 7.26 ppm. The spectrum confirms the formation of N-dodecyl-3-oxoquinuclidinium bromide, showing characteristic downfield resonances of the quinuclidinium scaffold at δ 4.68 ppm for H-2 and δ 4.15–3.98 ppm for H-6/H-8, together with the N-alkyl methylene signal at δ 3.79–3.73 ppm. Additional quinuclidine ring protons are observed between δ 2.87 and 2.32 ppm, while the dodecyl chain is represented by methylene resonances at δ 1.85–1.28 ppm and a terminal methyl triplet at δ 0.89 ppm. The observed chemical shifts and signal integrations are consistent with the proposed QO-C$_{12}$ structure and support the high spectral purity of the synthesized compound. **Abbreviations**: $CDCl_3$, deuterated chloroform; $CHCl_3$, chloroform; MHz, megahertz; NMR, nuclear magnetic resonance; ppm, parts per million; QO-C$_{12}$, N-dodecyl-3-oxoquinuclidinium bromide.

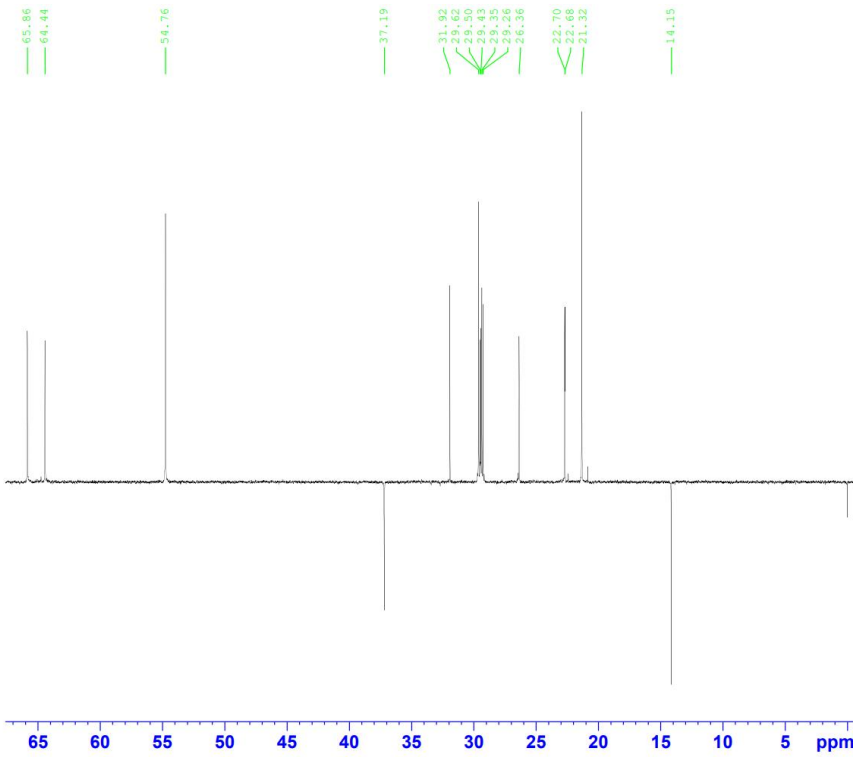


Figure S2. ^{13}C NMR spectrum of QO-C$_{12}$. Representative ^{13}C NMR spectrum of QO-C$_{12}$ recorded at 150 MHz in $CDCl_3$ at 298 K, with chemical shifts referenced to $CDCl_3$ at δ 77.16 ppm. The spectrum supports the proposed structure of N-dodecyl-3-oxoquinuclidinium bromide, showing the characteristic carbonyl carbon resonance at δ 201.3 ppm, quinuclidinium ring carbon signals at δ 65.9, 64.4, 54.8, 37.2, and 21.3 ppm, and alkyl-chain carbon resonances between δ 31.9 and 14.2 ppm. The observed carbon signals are consistent with successful N-alkylation of quinuclidin-3-one and confirm the structural identity and spectral purity of QO-C$_{12}$. **Abbreviations**: $CDCl_3$, deuterated chloroform; MHz, megahertz; NMR, nuclear magnetic resonance; ppm, parts per million; QO-C$_{12}$, N-dodecyl-3-oxoquinuclidinium bromide.

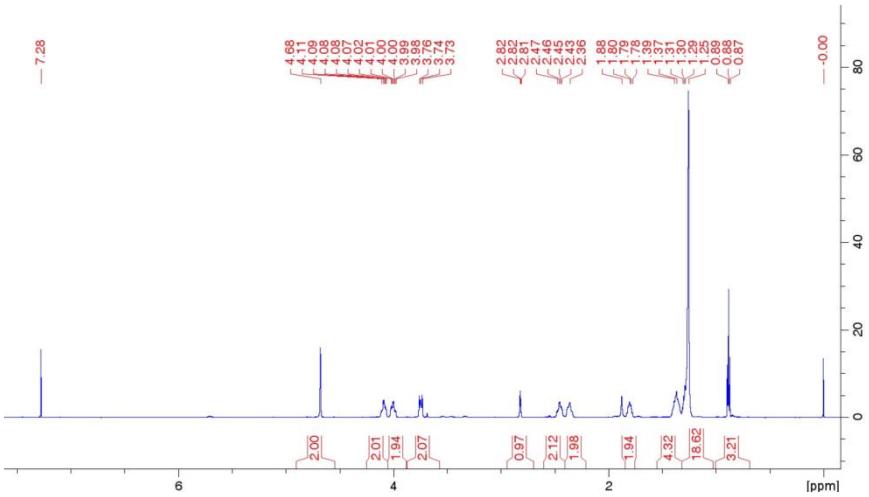


Figure S3. ^{1}H NMR spectrum of QO-C$_{14}$. Representative ^{1}H NMR spectrum of N-tetradecyl-3-oxoquinuclidinium bromide recorded at 600 MHz in $CDCl_3$ at 298 K. The spectrum shows the expected proton resonances of the quinuclidin-3-one core and tetradecyl chain, including signals assigned to H-2 at δ 4.68 ppm, quinuclidinium ring protons between δ 4.11–2.36 ppm, N-alkyl methylene protons at δ 1.88–1.78 ppm, the long-chain methylene envelope centered at δ 1.29 ppm, and the terminal methyl triplet at δ 0.88 ppm. Chemical shifts are referenced to residual $CHCl_3$ at δ 7.26 ppm. The spectrum confirms the identity and high spectral purity of QO-C$_{14}$ (M_r = 402.5). **Abbreviations**: $CDCl_3$, deuterated chloroform; $CHCl_3$, chloroform; M_r, relative molecular mass; NMR, nuclear magnetic resonance; ppm, parts per million; QO-C$_{14}$, N-tetradecyl-3-oxoquinuclidinium bromide.

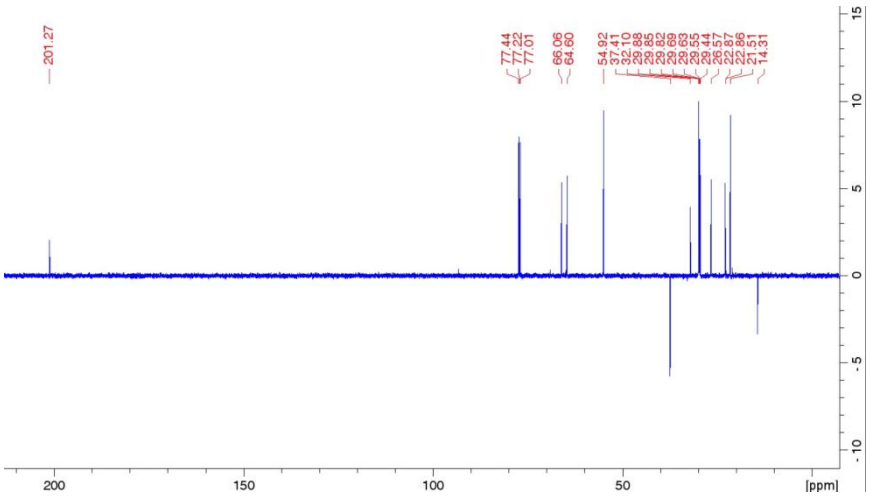


Figure S4. ^{13}C NMR spectrum of QO-C$_{14}$. Representative ^{13}C NMR spectrum of N-tetradecyl-3-oxoquinuclidinium bromide recorded at 150 MHz in $CDCl_3$ at 298 K. The spectrum displays the characteristic carbon resonances of the quinuclidin-3-one scaffold and tetradecyl side chain, including the carbonyl carbon signal at δ 201.3 ppm, signals attributable to the quinuclidinium ring carbons in the δ 66.1–21.5 ppm region, and the alkyl-chain carbons between δ 32.1 and 14.3 ppm. Chemical shifts are referenced to $CDCl_3$ at δ 77.16 ppm. The spectrum is consistent with the proposed structure and supports the identity and high spectral purity of QO-C$_{14}$ (M_r = 402.5). **Abbreviations**: $CDCl_3$, deuterated chloroform; M_r, relative molecular mass; NMR, nuclear magnetic resonance; ppm, parts per million; QO-C$_{14}$, N-tetradecyl-3-oxoquinuclidinium bromide.

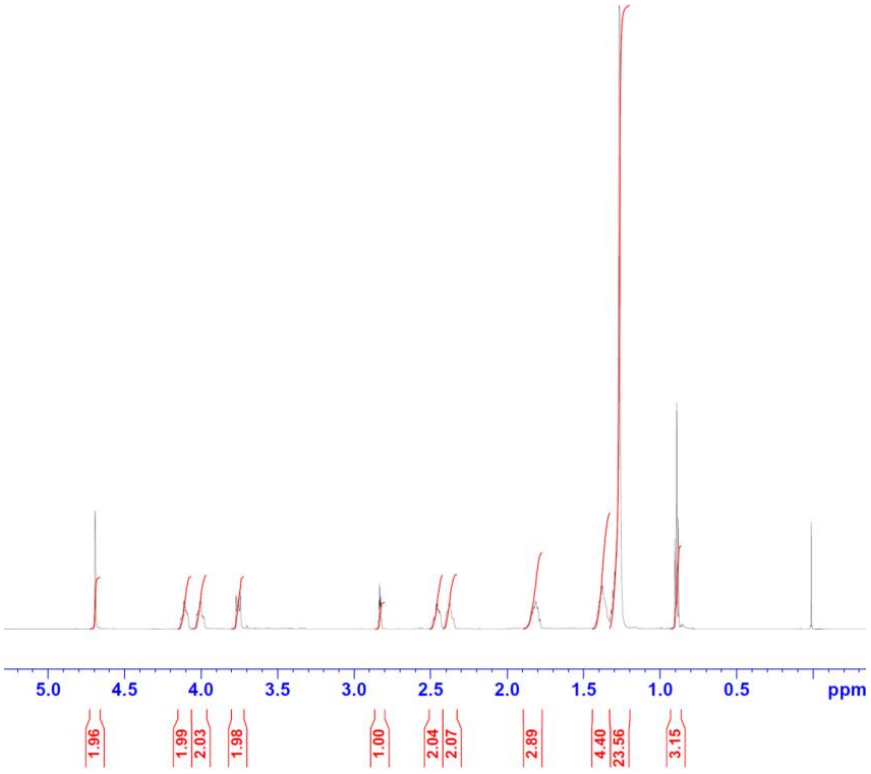


Figure S5. ^{1}H NMR spectrum of QO-C$_{16}$. Representative ^{1}H NMR spectrum of N-hexadecyl-3-oxoquinuclidinium bromide recorded at 600 MHz in $CDCl_3$ at 298 K. The spectrum exhibits the expected proton resonances for the quinuclidin-3-one core and the hexadecyl substituent, including the singlet for H-2 at δ 4.70 ppm, multiplets assigned to H-8 and H-6 at δ 4.15–4.09 and 4.03–3.95 ppm, respectively, the N-alkyl methylene protons at δ 3.77–3.71 ppm, the H-4 signal at δ 2.82 ppm, and resonances corresponding to H-7 and H-5 at δ 2.49–2.42 and 2.40–2.30 ppm. Signals of the alkyl chain are observed at δ 1.87–1.76 ppm (H-2′), 1.42–1.31 ppm (H-3′, H-4′), 1.28 ppm (H-5′–H-15′), and 0.89 ppm (H-16′). Chemical shifts are referenced to residual $CHCl_3$ at δ 7.26 ppm. The spectrum confirms the proposed structure and high spectral purity of QO-C$_{16}$ (N-hexadecyl-3-oxoquinuclidinium bromide; M_r = 430.5). **Abbreviations**: $CDCl_3$, deuterated chloroform; $CHCl_3$, chloroform; M_r, relative molecular mass; NMR, nuclear magnetic resonance; ppm, parts per million; QO-C$_{16}$, N-hexadecyl-3-oxoquinuclidinium bromide.

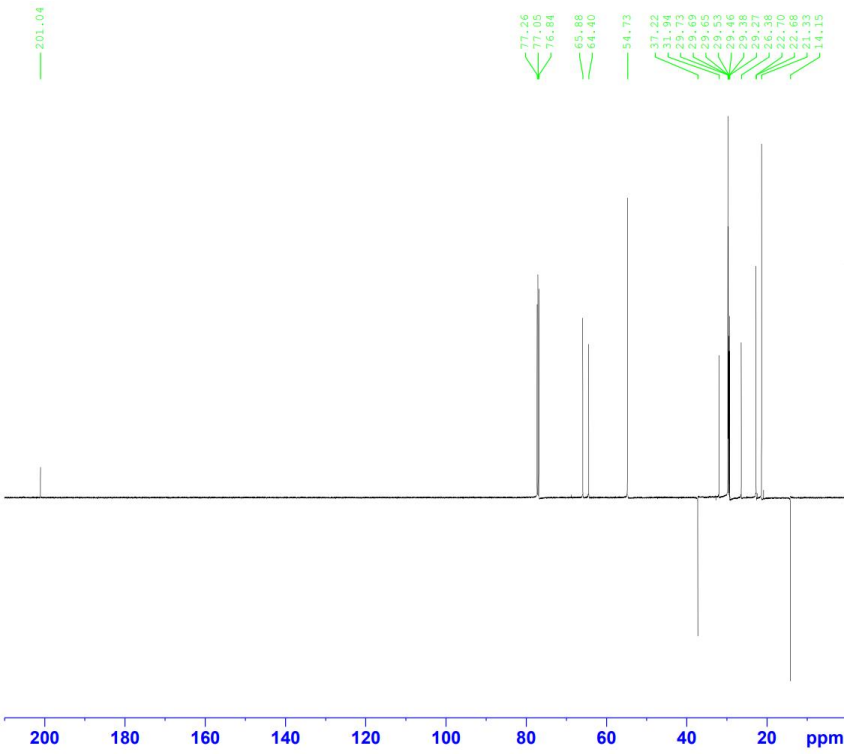


Figure S6. ^{13}C NMR spectrum of QO-C$_{16}$. Representative ^{13}C NMR spectrum of N-hexadecyl-3-oxoquinuclidinium bromide recorded at 150 MHz in $CDCl_3$ at 298 K. The spectrum shows the expected carbon resonances of the quinuclidin-3-one scaffold and hexadecyl substituent, including the carbonyl carbon at δ 201.0 ppm, quinuclidinium ring carbons at δ 65.9, 54.7, 37.2, and 21.3 ppm, and alkyl-chain carbons distributed between δ 31.9 and 14.2 ppm. Chemical shifts are referenced to $CDCl_3$ at δ 77.16 ppm. The spectral profile is consistent with the proposed structure and supports the identity and high spectral purity of QO-C$_{16}$ (N-hexadecyl-3-oxoquinuclidinium bromide; M_r = 430.5). **Abbreviations**: $CDCl_3$, deuterated chloroform; M_r, relative molecular mass; NMR, nuclear magnetic resonance; ppm, parts per million; QO-C$_{16}$, N-hexadecyl-3-oxoquinuclidinium bromide.

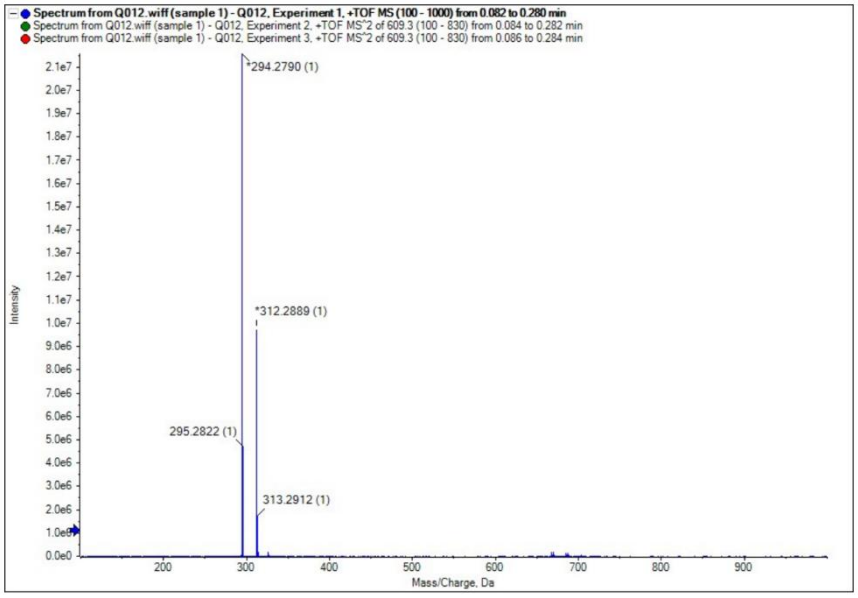


Figure S7. QTOF HRMS spectrum of QO-C$_{12}$ (ESI$^+$). Representative high-resolution QTOF mass spectrum of QO-C$_{12}$ acquired in positive electrospray ionization mode. The spectrum shows a dominant ion at *m/z* 294.2790, corresponding to the molecular cation [M]$^+$ of QO-C$_{12}$, in agreement with the calculated exact mass for $C_{19}H_{36}NO^+$ (294.2791). The minimal mass deviation (0.34 ppm) confirms the elemental composition of the analyte and supports the identity and high purity of QO-C$_{12}$. **Abbreviations**: ESI, electrospray ionization; HRMS, high-resolution mass spectrometry; *m/z*, mass-to-charge ratio; ppm, parts per million; QO-C$_{12}$, N-dodecyl-3-oxoquinuclidinium bromide; QTOF, quadrupole time-of-flight.

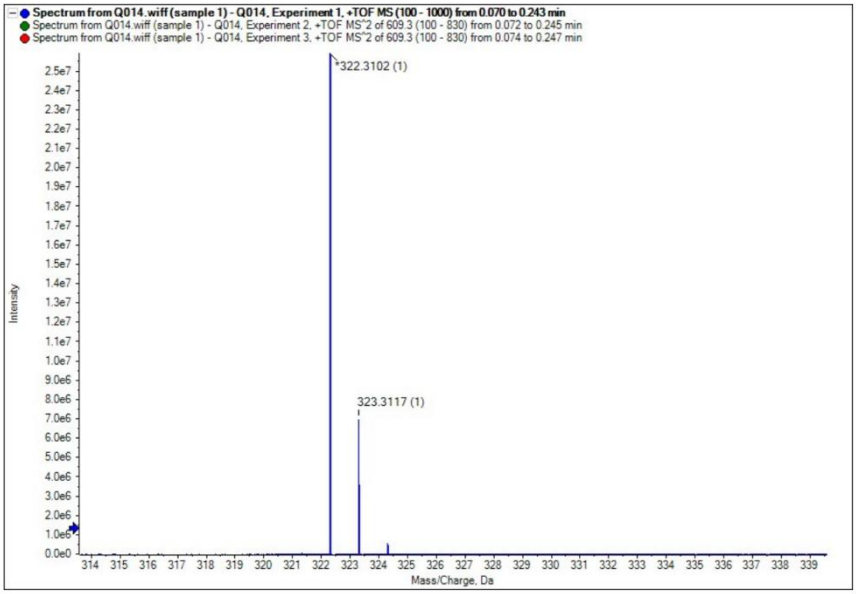


Figure S8. QTOF HRMS spectrum of QO-C$_{14}$ (ESI$^+$). Representative high-resolution QTOF mass spectrum of QO-C$_{14}$ acquired in positive electrospray ionization mode. The spectrum shows a dominant ion at *m/z* 322.3102, corresponding to the molecular cation $[M]^+$ of QO-C$_{14}$, in agreement with the calculated exact mass for $C_{21}H_{40}NO^+$ (322.3104). The low mass deviation (0.62 ppm) confirms the elemental composition of the analyte and supports the identity and high purity of QO-C$_{14}$. **Abbreviations**: ESI, electrospray ionization; HRMS, high-resolution mass spectrometry; *m/z*, mass-to-charge ratio; ppm, parts per million; QO-C$_{14}$, N-tetradecyl-3-oxoquinuclidinium bromide; QTOF, quadrupole time-of-flight.

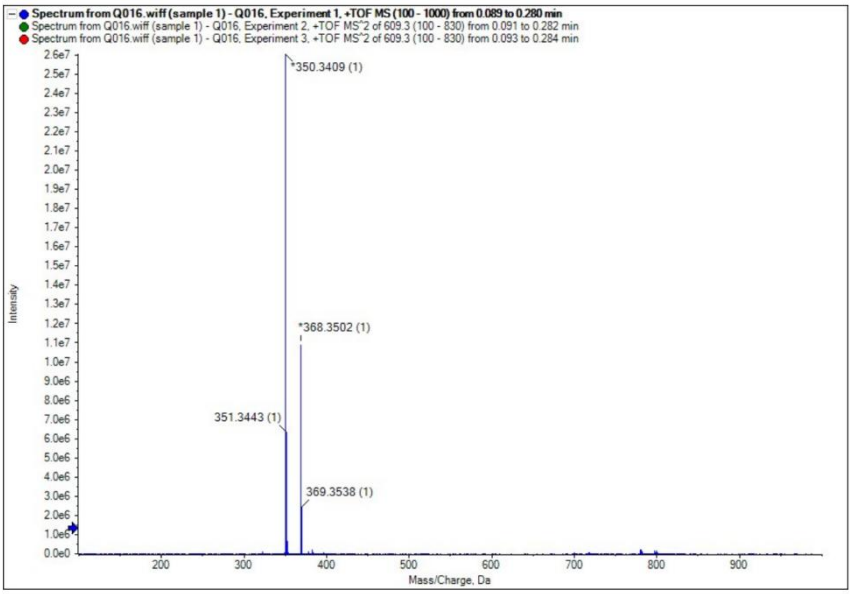


Figure S9. QTOF HRMS spectrum of QO-C$_{16}$ (ESI$^+$). Representative high-resolution QTOF mass spectrum of QO-C$_{16}$ acquired in positive electrospray ionization mode. The spectrum shows a dominant ion at *m/z* 350.3409, corresponding to the molecular cation [M]$^+$ of QO-C$_{16}$, in agreement with the calculated exact mass for $C_{23}H_{44}NO^+$ (350.3417). The observed mass accuracy, with a mass error of 2.28 ppm, confirms the elemental composition of the analyte and supports the identity and high spectral purity of QO-C$_{16}$. **Abbreviations**: ESI, electrospray ionization; HRMS, high-resolution mass spectrometry; *m/z*, mass-to-charge ratio; ppm, parts per million; QO-C$_{16}$, N-hexadecyl-3-oxoquinuclidinium bromide; QTOF, quadrupole time-of-flight.